Materials Advances

ROYAL SOCIETY OF CHEMISTRY

PAPER

View Article Online
View Journal | View Issue

Cite this: *Mater. Adv.*, 2024, 5, 1119

Sensing and conversion of carbon dioxide to methanol using Ag-decorated zinc oxide nanocatalyst

Sheraz Ahmad,[a] Akbar Hussain,[a] Shabeer Ahmad Mian, *[a] Gul Rahman, [b] Shaukat Ali [b] and Joonkyung Jang *[c]

The catalytic hydrogenation of CO_2 to methanol, which is one of the most important byproducts, has been studied using density functional theory simulations. The chemisorption of silver (Ag) atoms on the ZnO nanocage surface significantly narrowed the bandgap from 4.05 to 1.27 eV and altered the overall optoelectronic and catalytic properties of the nanocage. We introduced a successful two step activation and conversion of carbon dioxide into methanol and water. The high performance of the Ag-decorated ZnO catalyst activated the CO_2 gas owing to its chemisorbed nature. At this stage, three H_2 molecules were incorporated to surround the chemisorbed CO_2 gas, which converted it to methanol (CH_3OH) and water molecules with an enhanced sensitivity of 70%. This demonstrates maximum sensing response up to 54% at room temperature (300 K), which further lowered the bandgap from 1.23 to 0.70 eV. The calculated recovery time of the Ag-decorated ZnO sensor was 5.06×10^{-09} s, indicating its outstanding optical characteristics, strong chemical stability, and high electron mobility. The adsorption energies of the Ag-decorated and activated CO_2-adsorbed ZnO complexes were found to be −1.76, and −0.28 respectively, indicating a thermodynamically stable configuration. This study focuses on CO_2 activation, advances the catalytic hydrogenation of CO_2 to methanol to develop high-performance catalysts with enhanced sensing responses and recovery times, and provides insight into the reaction mechanisms.

Received 14th September 2023,
Accepted 11th December 2023

DOI: 10.1039/d3ma00705g

rsc.li/materials-advances

1. Introduction

Global warming and climate change are the most challenging and serious threats to humanity in the 21st century.[1] The amount of carbon dioxide (CO_2) in the Earth's atmosphere has increased by almost 75% owing to the industrial and transportation revolutions.[2,3] CO_2 gas enters the Earth's atmosphere both from natural (volcanic eruptions and respiration) and anthropogenic activities (incomplete combustion of fossil fuels in power plants, industries, and transportation and biomass burning).[4] Environmental pollutants from different sources pollute water, air, rivers, and the ecosystem, leaving unsafe and poor-quality air for breathing.[5,6] This has adverse effects on the health of inhabitants, rainfall, and the concentration of solar radiation.[7,8] Excessive CO_2 levels above 40 000 ppm can cause diseases such as respiratory infections, pulmonary diseases, heart diseases, and lung cancer.[9–12]

Moreover, CO_2 affects the climatic conditions in two ways:[13,14] It directly absorbs solar rays and heats the Earth's atmosphere, and it indirectly prolongs the lifespan of clouds.[15,16] It is a highly absorbing carbon-containing gas that contributes to global climate change.[17,18] The atmospheric effluents emerge into the Earth's atmosphere as carbon monoxide owing to the incomplete combustion of gasoline and fossil fuels in automobiles and various industries.[19] These primary effluents interact chemically with existing atmospheric constituents, resulting in secondary environmental effluents that lead to global warming.[20] In fact, in 2022, CO_2 emissions from anthropogenic activities reached a new high of approximately 33.8 billion tons.[21] Therefore, converting CO_2 into some useful by-products *via* the reaction of $CO_2 + 3H_2 \rightarrow CH_3OH + H_2O$ to reduce its harmful environmental impact is crucial.[22,23] In light of the aforementioned threats posed by CO_2 gas, methods must be developed for sensing, monitoring, and controlling the emission of contaminants polluting the Earth's atmosphere. In the last 20 years, researchers have attempted to develop heterogeneous catalysts for CO_2 hydrogenation to methanol as a byproduct.[24] Methanol is widely used as a fuel and is an essential chemical feedstock in the synthesis of chemicals and fuels.[25]

[a] *Department of Physics, University of Peshawar, Pakistan. E-mail: shabeerahmad@uop.edu.pk*
[b] *Institute of Chemical Sciences, University of Peshawar, Pakistan*
[c] *Department of Nano energy Engineering, Pusan National University, Republic of Korea. E-mail: jkjang@pusan.ac.kr*

Zinc oxide (ZnO) is one of the materials that can be used as both a gas sensor and a catalyst to produce useful byproducts.[26] ZnO is a white, water-insoluble n-type inorganic metal oxide semiconductor with a wide bandgap (3.37 eV) and a large exciton binding energy (60 meV) at room temperature and belongs to groups II–VI.[27] It is a chemically and thermally stable material possessing a hexagonal structure with lattice parameters of $a = b = 3.250$ Å and c = 5.206 Å.[28] A good sensor has good range, precision, repeatability, stability, sensitivity, and response time.[29] It is synthesized in different forms, such as nanowires, nanotubes, nanosheets, and nanoparticles.[30] In this study, the most favorable and stable semiconductor structure in the form of a nanocage with the formula $(XY)_n$ was developed, where X and Y represent metallic and nonmetallic elements, respectively, and n represents the number of atoms (12 in this case).[31] Each $(XY)_{12}$ nanocage is a compact octahedron with eight hexagons and six tetragons and it is one of the most investigated nanoclusters for gas sensing and heterogeneous catalysis.[32] The $(ZnO)_{12}$ nanocage has attracted considerable interest owing to its semiconducting, piezoelectric, and pyroelectric properties, making it suitable for applications in photovoltaic cells, optical sensitizers, sensors, hydrogen storage, and nanocarriers in biomedicine.[33] Pristine nanoclusters exhibit poor interaction with various gas molecules and are thus ineffective sensors.[34] To address these limitations, a few techniques, such as defect generation in the nanomaterial framework, impurity atom doping, surface modification, and decoration, have been developed.[35,36]

Decorating pristine nanocages with transition metals significantly reduces their resistance and improves their sensing, catalytic, electronic, and optical properties. $(ZnO)_{12}$ is a typical nanostructure that has been extensively investigated as a gas sensor owing to its outstanding electrical characteristics, strong chemical stability, and high electron mobility. It can be used in biological and environmental applications because of its superior catalytic activity and high surface-to-volume ratio. This study aims to investigate the effect of Ag on the electronic and optical properties of ZnO for the detection and conversion of CO_2 into useful chemicals. The bandgap of ZnO was reduced with Ag decoration, which ultimately enhanced its electronic conductivity compared to pristine ZnO. The results demonstrated that silver-decorated ZnO has the potential to detect CO_2 gas and can successfully convert it into value-added methanol, which is used as a fuel in methanol fuel cells.

2. Computational details

In this study, pristine and Ag-decorated ZnO nanoclusters were explored using DFT employed in Spanish Initiative for Electronic Simulations with Thousands of Atoms (SIESTA).[37] First, a ZnO nanocage with 12 atoms of each element was designed and optimized using a $3 \times 3 \times 1$ k-point grid. An energy cutoff of 200 Ry and a $6 \times 6 \times 6$ k-point grid were used for the optoelectronic property calculations.[38] For tight convergence, the self-consistent field and atomic force of 10^{-6} eV and 0.002 eV Å^{-1}, respectively, were considered within the conjugate-gradient approximation. Evidently, GGA underestimates[39] and LDA overestimates the bandgap energy,[40] whereas the hybrid DFT improperly represents the Coulombic interactions in 'd' and certain other high-energy states in the case of transition metals.[41] Therefore, a hybrid DFT with 25% LDA and 75% GGA, along with the Hubbard parameter ($U = 11$) for transition metals,[36,42–44] was considered for the accurate calculations. In addition, all geometries were optimized using GGA with the Revised Perdew–Burke–Ernzerhof (RPBE) exchange correlation.[45] For each atom of the ZnO nanocage, the pseudo-atomic orbital (PAO) basis set was used, followed by the double zeta potential (DZP).[37,46]

3. Results and discussion

3.1. Geometrical analysis of pristine and Ag-decorated ZnO nanocages

The zinc oxide nanocage, consisting of 24 atoms and forming a compact octahedron with eight hexagons and six tetragons, was investigated using DFT. Two distinct Zn–O bond lengths inside the nanoclusters were observed: a bond length of 1.901 Å between the two hexagon rings and 1.972 Å between a tetragon and a hexagon ring, which is in agreement with the experimental ZnO nanocluster bonds.[36,47] The angles of the four- and six-membered rings of the $(ZnO)_{12}$ nanocage varied from 90.907° to 87.043° and 126.043° to 107.847°, respectively. At the center of the tetragonal ring of the $(ZnO)_{12}$, Ag atoms were adsorbed, indicating the most stable $(ZnO)_{12}$/Ag structure, as shown in Fig. 1(b). The chemisorbed Ag atom formed two strong, distinct bonds with the Zn atom with bond lengths of 2.667 and 2.650 Å (Fig. (1b)), which are consistent with the literature results.[48,49] The adsorption energy of the Ag-decorated $(ZnO)_{12}$ nanocage was ~ -1.76 eV, indicating an exothermic process.[49] Due to the instability in the HOMO level of ZnO, Ag adsorption significantly narrowed the bandgap energy (E_g) of pristine ZnO from 4.05 to 1.27 eV, as depicted in Table 1.

CO_2 is a highly stable molecule with strong C═O bonds (bond energy of 7.8 eV) compared to C–C (3.48 eV) and C–O (3.38 eV); hence, its reduction is very challenging. Breaking the C═O bond during photocatalytic reduction requires a significant amount of energy. Herein, using Ag as a catalyst, CO_2 was activated and efficiently converted to methanol and water. The angle of O═C═O drastically changed, and one C═O double bond of the activated CO_2 converted to a single C–O bond. Subsequently, the activated CO_2 was hydrogenated, resulting in the targeted products, *i.e.*, methanol and water (Fig. 1(c)), with C═O stretched from 0.029c to 8.862 Å in the adsorbed state. The adsorption of CO_2 molecules on the Ag-decorated ZnO surface was investigated using the parallel orientation of the CO_2 molecules, and strong adsorption was observed.[47,50] The CO_2 adsorption reduced the angle from 180° to 162.28° and one double bond to a single bond, as shown in Fig. 1c. Furthermore, the CO_2 adsorption on the Ag-decorated ZnO lengthened the bond between Ag and the surface from 2.667 and 2.65 to 2.719 and 2.694 Å, respectively. This indicates that CO_2 attempted to extract Ag atoms from the ZnO surface.

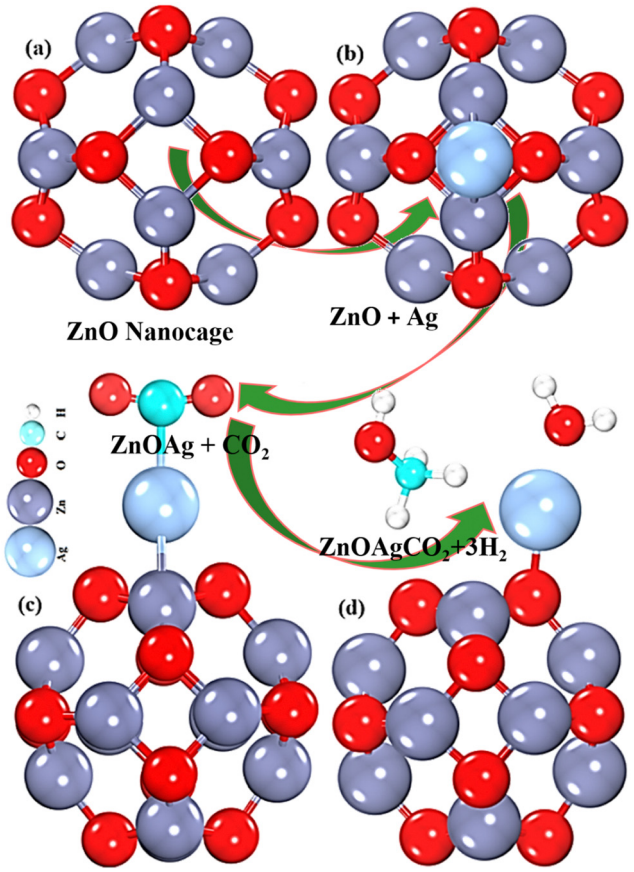

Fig. 1 Optimized geometry of (a) pristine, (b) Ag-decorated ZnO (top view), (c) CO_2-adsorbed Ag-decorated ZnO nanoclusters, and (d) byproduct (methanol + H_2O).

Table 1 Bandgap energy (E_g), adsorption energy (E_{ad} eV), and sensitivity (S) of the pristine, Ag-decorated, and CO_2-adsorbed ZnO derivatives

Material	E_{ad}	E_{LUMO}	E_{HOMO}	E_g	Sensitivity %
ZnO		1.92	−2.13	4.05	—
ZnO/CO_2	—	1.28	−2.85	4.13	—
ZnO + Ag	−1.76	1.28	0.01	1.27	—
AgZnO + CO_2	−0.28	1.23	−0.00	1.23	70
AgZnOCO_2 + $3H_2$	−0.061	0.75	0.05	0.70	—

Additionally, the binding energy of CO_2 with the Ag-decorated ZnO nanocage confirmed CO_2 activation. The negative adsorption energy E_{ad} of −0.28 eV validates the thermodynamic favorability of adsorption, which is consistent with the findings of Sikam *et al.*[50,51]

The conversion of CO_2 into methanol (CH_3OH) is in high industrial demand because it is a clean and sustainable energy source that can meet the increasing energy demands. To achieve this, we surrounded activated CO_2 with three H_2 molecules and observed their interactions. The three H_2 molecules were found to strongly interact with the activated CO_2 and form CH_3OH and H_2O, which were successfully detached from the catalyst (Ag-decorated ZnO) *via* the chemical reaction:

$$CO_2 + 6e^- + 6H^+ \rightarrow CH_3OH + H_2O \text{ (Fig. 1(d))}.$$

The desorption/formation energy[52,53] of the product methanol (CH_3OH) is calculated to be −2.23 eV, which is more negative than that of the previously reported studies,[54] thus indicating an exothermic reaction and the superiority of the ZnO nanocage for methanol production.

The iterative optimizations of both the pure and Ag-decorated ZnO nanocages in terms of energy and cell volume are shown in Fig. 2(a) and (b). Optimization of the complete reaction revealed that the variation in the cell volume and energy of both compositions attained the ground state with the minimum optimized energy and geometric stability. The volume expansion of the $(ZnO)_{12}$ nanocage[55] caused by Ag adsorption is shown in Fig. 2(b). The system tends to minimize its free energy to reach the maximum possible stable state.[56] The addition of further reactants into the system resulted in a more negative value of free energy, suggesting a stronger contact between the activated CO_2 complex and the three H_2 molecules. This implies that the activated CO_2 reacted with H_2 gas on the nanocage surface and finally detached from the surface after the formation of methanol and water molecules, resulting in cell volume contraction, as shown in Fig. 2(c) and (d).

3.2. Calculation of adsorption energy of the CO_2 and complex

The adsorption energy for the complete reaction pathway involving the ZnO nanocage, silver, CO_2, adsorption, and H_2 gas interaction with activated CO_2 is described by the following equation:[36]

$$E_{Ad} = E_{ZnOAgCO_2+3H_2} - E_{ZnOAgCO_2} - E_{3H_2} \quad (1)$$

Where $E_{ZnOAgCO_2+3H_2}$ corresponds to the energy of the Ag-decorated ZnO nanocage on which the CO_2 molecule was activated in the presence of H_2 gas. The negative adsorption energy indicates an exothermic reaction,[57] and the catalytic role of Ag-decorated ZnO. Therefore, AgZnO plays a catalytic role in CO_2 adsorption.[58] The adsorption energies for the Ag-decorated ZnO and CO_2 adsorbed AgZnO were found to be −1.76, and −0.28 eV, while the desorption energy of the CH_3OH was calculated to be −2.23 eV, respectively. Higher negative adsorption energy values (shown in Table 1) indicate stronger stability.[59]

3.3. Molecular orbitals analysis

The energy bandgap (E_g) is determined by the energy difference using eqn (2),[60,61] which provides information about the kinetic stability and chemical reactivity of the system. A molecule with a smaller energy gap is more polarizable and typically has high chemical reactivity and low kinetic stability.[62]

$$E_g = E_{LUMO} - E_{HOMO} \quad (2)$$

where E_{LUMO} and E_{HOMO} are the energies of the HOMO and LUMO.

The electronic band structures of all the reactants are shown in Fig. 2(a)–(d) The E_g of 4.05 eV for pure ZnO (Fig. 2(a)) agreed well with previously reported theoretical results.[35,61,63] CO_2

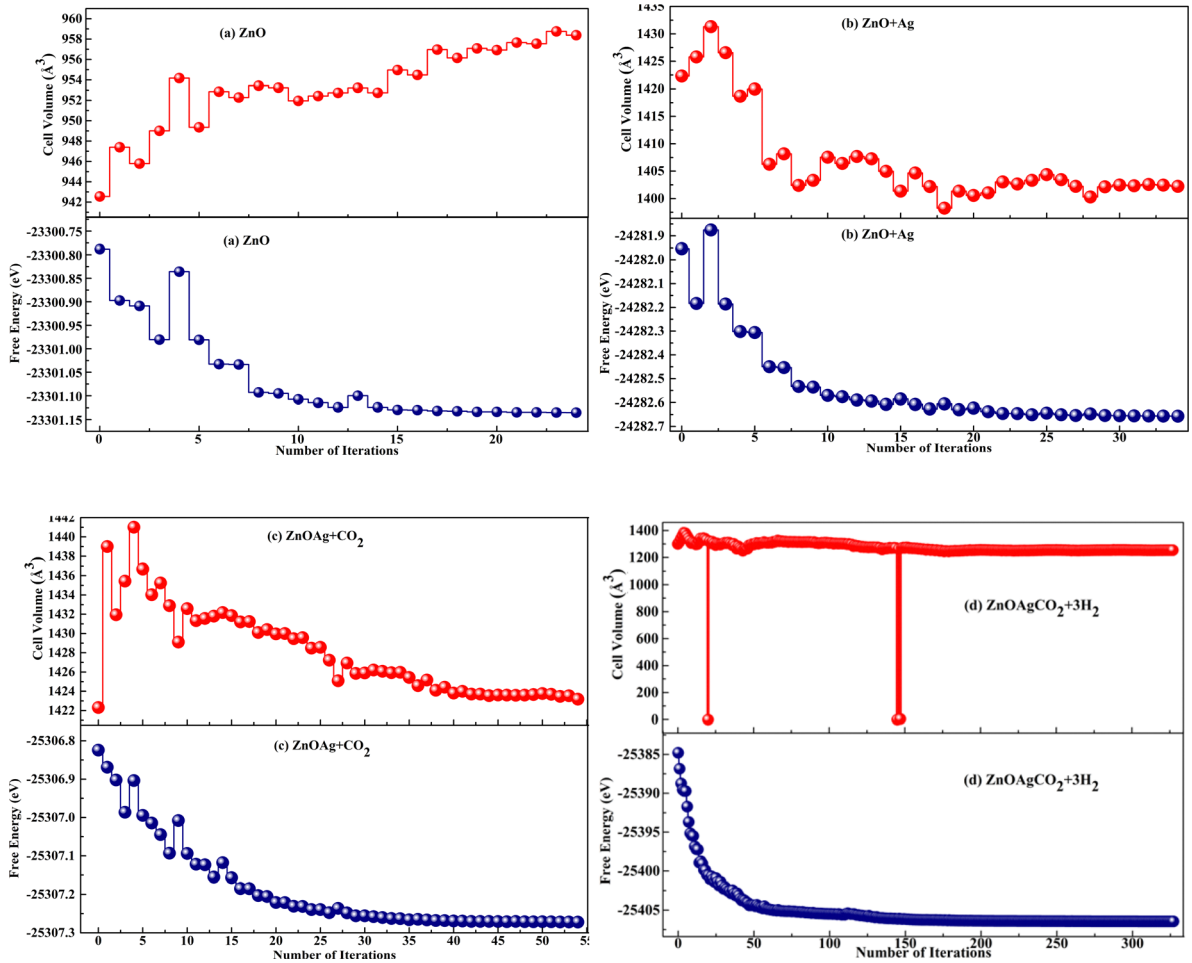

Fig. 2 (a)–(d) Plots of free energy and volume *vs.* the number of iterations for the complete reaction pathway involving pure and Ag-decorated ZnO nanocages.

adsorption on the pristine nanocage exhibited a negligible impact on the bandgap of the nanocage; therefore, its sensing response towards CO_2 was very poor. Initially, we placed CO_2 on the pristine ZnO nanocage at 2.6 Å distance; however, after optimization, the distance increased, indicating the inert nature of the ZnO nanocage towards CO_2 (Fig. 3(a)). The E_g increased from 4.05 to 4.13 eV (Table 1), confirming that CO_2 gas sensing using a pristine ZnO nanocage is not possible.

Adsorption of the Ag on the pristine nanocage reduced the E_g value from 4.05 to 1.27 eV, indicating improved conductivity. The positions of the E_{HOMO} and E_{LUMO} levels of the Ag-decorated ZnO nanocage demonstrated its reduction capability. Furthermore, the CO_2 adsorption altered the E_g to the lower infrared and visible regions, as shown in Fig. 4(c). Moreover, the impact of H_2 molecules on the electronic properties of the nanocage was investigated. H_2 was found to narrow the bandgap to 0.70 eV (Fig. 4(d)), owing to the generation of intermediate energy states near the Fermi level.

Fig. 5 shows the projected density of states (PDOS) for all the ZnO compositions. In pristine ZnO, the E_{LUMO} was mostly composed of O-2p orbitals, followed by Zn-3d, whereas the E_{HOMO} was dominated by Zn-4s and O-2p. Similarly, the valence band of the Ag-incorporated ZnO nanocage was dominated by the Ag-5s states compared to Zn-4s and O-2p, which are very close to the Fermi line (Fig. 5(b)). The highly occupied energy levels resulted in enhanced optical properties of the material and a drastic transition of electrons from the valence band to the conduction band.[59]

Fig. 5(c) shows the PDOS of the $AgZnOCO_2$ complex with newly occupied states formed inside the E_g of AgZnO because of the contribution of the O-2s and O-2p states. Furthermore, the addition of the three H_2 molecules to the pre-adsorbed CO_2 complex weakened the O–O bond and led to methanol formation owing to the overlapping of the H-1s, O-2s, and C-2s states. The binding energies of the final products, viz., methanol, water, and Ag-decorated ZnO, indicated that the reaction was favorable at room temperature. The PDOS plots for all configurations shown in Fig. 5(a)–(d) confirmed the sensitivity of CO_2 towards the Ag-decorated nanocage by reducing the E_g value, thereby significantly enhancing the conductivity. Therefore, the Ag-decorated ZnO nanocage has the potential to convert CO_2 gas directly into electrical signals and can therefore be used in CO_2 sensors.[60]

3.4. Sensitivity of the Ag-decorated ZnO nanocage

The sensitivity is defined as the ratio between the difference in the bandgap of Ag-decorated ZnO (E_{g1}) and the CO_2 adsorbed on it (E_{g2}).[35]

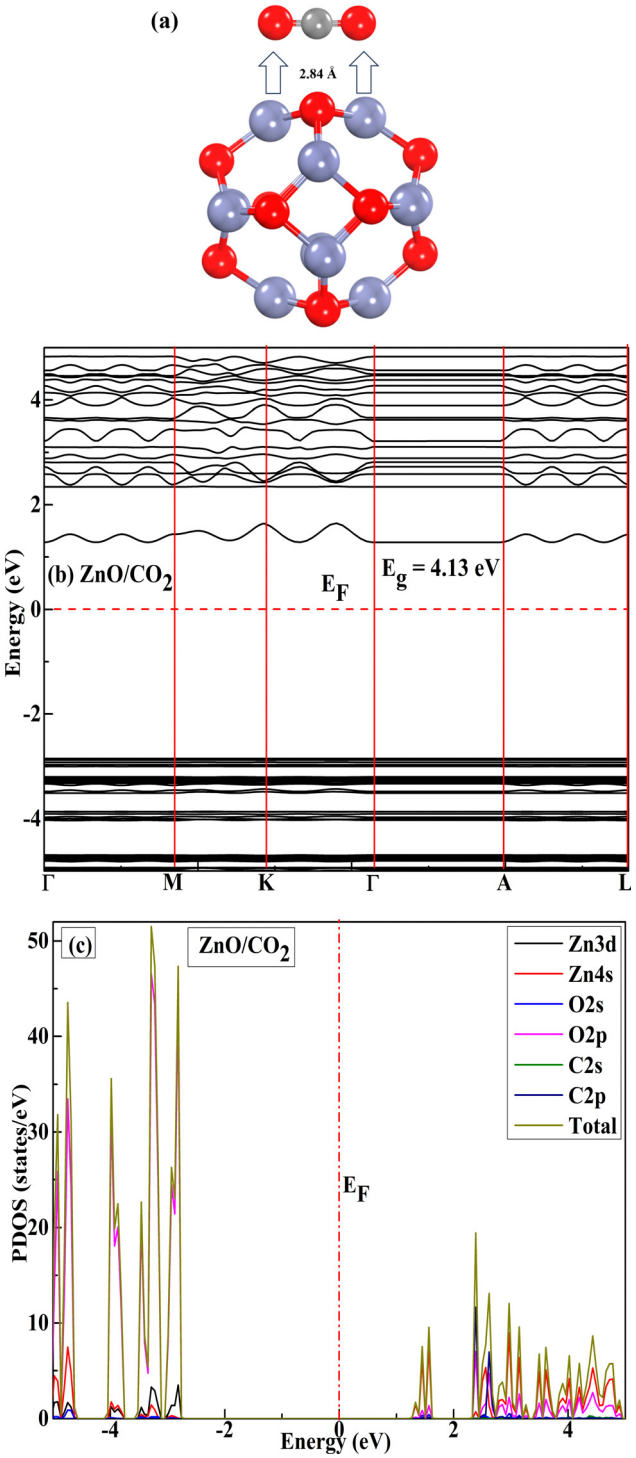

Fig. 3 Optimized geometry: (a) interaction of CO_2 with pristine ZnO, (b) and (c) portrayed the band gap and PDOS for the adsorbed CO_2 on the ZnO nanocage.

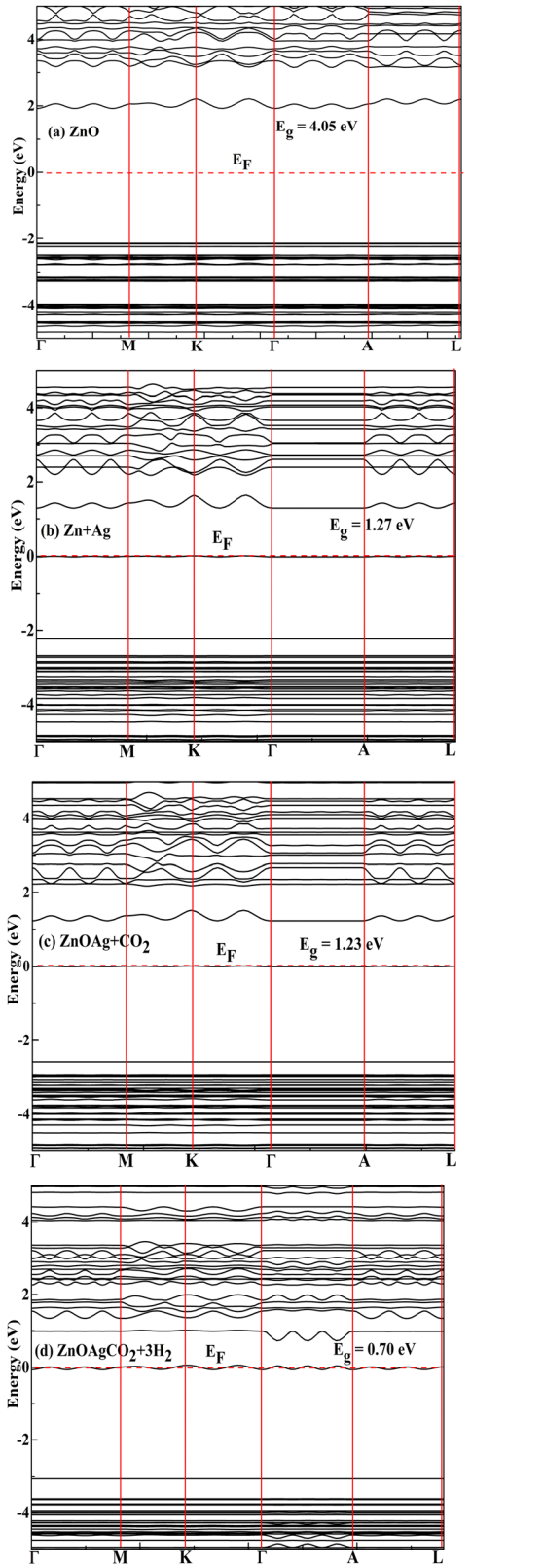

Fig. 4 Band structure of (a) pristine, (b) Ag-decorated, and (c) and (d) CO_2-adsorbed complexes on the Ag-decorated $(ZnO)_{12}$ nanoclusters.

$$S = \frac{(E_{g2} - E_{g1})}{E_{g1}} \quad (3)$$

Because there is a relationship between E_g and electrical conductance (σ), E_g can be used to test the sensitivity of E_g towards gas complexes. In the absence of transition metals, the sensitivity of the ZnO towards CO_2 gas was estimated to be approximately 2%, which was very low. However, after

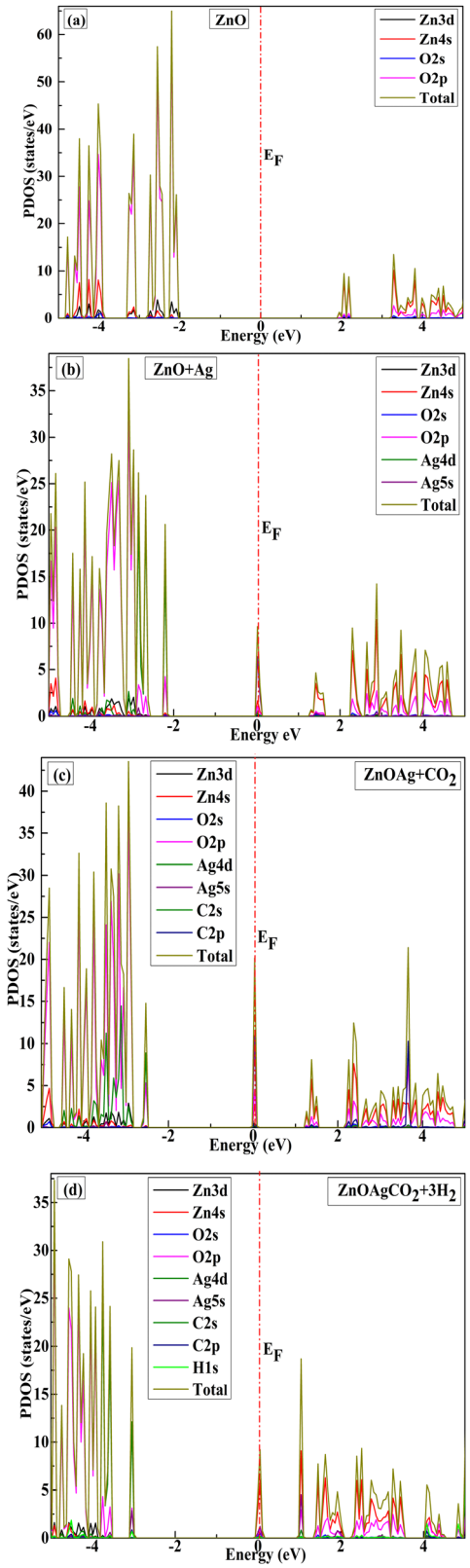

Fig. 5 Projected density of states of (a) pristine, (b) transition metal-decorated, and (c) and (d) CO_2-adsorbed complexes on the transition metal-doped (decorated) $(ZnO)_{12}$ nanocage.

decorating Ag on the nanocage surface, its sensitivity significantly increased to 70%. Table 1 lists the calculated values of sensitivity of various ZnO derivatives towards CO_2.[35,61]

3.5. Conductivity of the Ag-decorated ZnO nanocage

Variations in the bandgap change the conductivity of the material.[64] Our calculations revealed that the pure ZnO nanocage exhibited poor conductivity. The decoration of ZnO with Ag markedly enhanced its conductivity, as shown in Table 2. The pristine ZnO nanocage did not interact with CO_2 (Fig. 3(a)). The conductivities (σ) of the pure and Ag-decorated ZnO nanocages were calculated using eqn (4) and (5):[61]

$$\sigma \propto \exp(-E_g/2kT) \quad (4)$$

$$\sigma = AT^{3/2}\exp(-E_g/2kT) \quad (5)$$

where A (electrons m^{-3} $K^{-3/2}$) is a constant, and k is the Boltzmann constant. According to eqn (4), σ is inversely proportional to the bandgap (E_g) of the material. Thus, the Ag-decorated ZnO nanocage may transmit an electrical signal in the presence of CO_2 molecules in the environment where it is installed.

Experimentally, Han *et al.* demonstrated that in the absence of transition metals, the trend in conductivity, sensing response, and recovery time of the nanocage towards CO_2 gas was extremely low compared to the silver-decorated (ZnO) nanocage. This result was theoretically verified in this study at various temperatures listed in Table 2.[65,66]

The sensing response can be expressed by eqn (6).

$$SR\% = \frac{\left|\frac{1}{\sigma_{gas}} - \frac{1}{\sigma_{pure}}\right|}{\frac{1}{\sigma_{pure}}} = \left|\frac{\sigma_{pure} - \sigma_{gas}}{\sigma_{gas}}\right| \quad (6)$$

where SR represents a sensing response, σ_{pure} is the conductivity of the pure ZnO nanocage, and σ_{gas} is the conductivity of the gas adsorbed on the ZnO nanocage $(\Omega\ m)^{-1}$.

The adsorption of Ag on the ZnO surface greatly improved its conductivity compared to that of the bare nanocage at temperatures ranging from room temperature to high temperatures (Table 2).[66] As previously explored[35] and supported by our findings (Table 1), the bandgap of Ag-decorated ZnO further altered E_g after the adsorption of CO_2 gas on the ZnO surface. Gas molecule detection on a pristine ZnO surface was in a very depressed mode.

Table 2 Sensing response (SR%) recovery time after adsorption of CO_2 on an Ag-decorated ZnO nanocage at various temperatures (K)

System	Temperature	Sensing response	Recovery time
ZnOAg + CO_2	300	−54	5.06×10^{-09}
	320	−51.6	2.60×10^{-09}
	340	−49.5	1.41×10^{-09}
	360	−47.5	8.31×10^{-10}
	380	−45.7	5.17×10^{-10}
	400	−44	3.37×10^{-10}

3.6. Recovery time of the Ag-decorated ZnO nanocage

The time required by the sensor to return to its baseline or original position can be calculated using eqn (7):[60]

$$T = V_0^{-1} \exp(-E_{ad}/kT) \quad (7)$$

where V_0, T, and k represent the attempt frequency, temperature, and Boltzmann constant (8.61×10^{-05} eV), respectively. The calculated recovery time of CO_2 adsorption on the surface of the pristine and Ag-decorated ZnO nanocages is listed in Table 2.[67]

The $ZnOAgCO_2 + 3H_2$ complex demonstrated that the three H_2 molecules combine with the previously chemisorbed CO_2 gas by weakening and breaking the C=O double bond under the catalytic effect of the Ag-decorated ZnO nanocage to generate the useful product, methanol (CH_3OH), which is a renewable energy source for the following reaction:

$$CO_2 + 3H_2 \rightarrow CH_3OH + H_2O$$

3.7. Optical absorption and conductivity of the Ag-decorated ZnO nanocage

The pristine $(ZnO)_{12}$ nanocage exhibited absorption at 4.05 eV in the ultraviolet region, which is consistent with the experimental data[68] and correlates with maximal absorption occurring in the ultraviolet portion of the solar spectrum at an incident photon energy of 4.3 eV (~289 nm) (Fig. 6). After Ag adsorption, the optical mobility of the (ZnO) nanocage was enhanced. Bandgap engineering (surface modification by Ag) facilitated the nanoclusters to absorb more visible light, boosting electron–hole pair production for photocatalytic activity while reducing their recombination. The electromagnetic absorption spectrum was further improved when CO_2 and H_2 gas molecules were absorbed by the Ag-decorated ZnO nanocage, as shown in Fig. 6. Kumar *et al.* reported that a transition-metal-decorated ZnO nanocage exhibits a maximum response at 323 K.[49,69] Moreover, it exhibits a greenhouse effect because it absorbs infrared (IR) radiation from the Earth's surface.[70,71] Fig. 6 shows that CO_2 absorption is exceptionally high because of its massive emissions owing to the modern living standards of human beings.[72]

Fig. 7 shows the optical conductivities of all compositions. The conductivity of the pristine material is in accordance with the absorption spectrum. Upon Ag incorporation, when the photon energies exceeded 0.78 eV, optical conductivity was found to be dominant. After 3.44 eV, optical conductivity decreased gradually. Charge transfer from the valence band to the conduction band was accompanied by a sharp absorption peak at 360 nm, as verified by Bae *et al.*[73] Visible light-induced photocatalysis is particularly effective in the presence of carbon because it drives photoexcited electrons on the catalyst surface, separates photoelectrons and holes, and decreases the rate of electron–hole recombination.[74] Under visible-light irradiation, the Ag-decorated ZnO nanocage exhibited greater photocatalytic absorption, optical conductivity activity, and the highest efficiency compared to the pristine ZnO nanocage. Moreover, the CO_2 and complex adsorbed on the Ag-decorated (ZnO) exhibited improved photoconductivity in the visible-to-ultraviolet region. This was attributed to a redshift in band energy and absorption in the broad solar spectrum (360–1589 nm).

3.8. Quantum molecular description

Table 3 summarizes the quantum chemical properties of the pristine, Ag-decorated, and CO_2-adsorbed ZnO nanocage complexes, which provide information about the chemical reactivity of the gas molecules. The chemical behavior of the investigated gas complexes can be predicted using these properties.[75,76]

$$\text{Ionization energy (IE)} = -E_{HOMO} \quad (8)$$

$$\text{Electron affinity (Ea)} = -E_{LUMO} \quad (9)$$

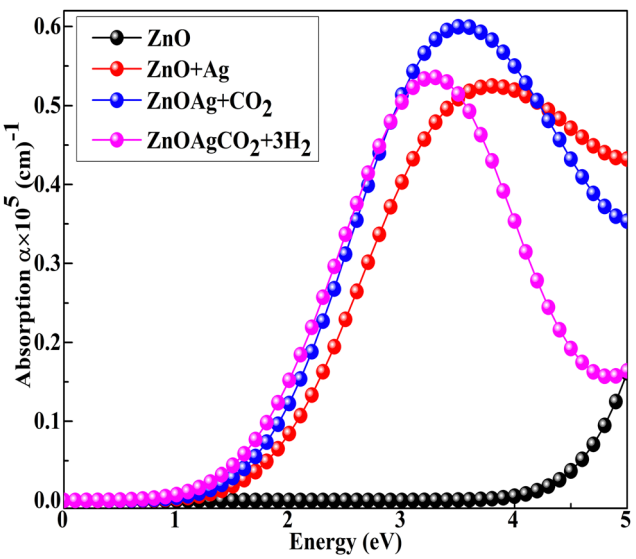

Fig. 6 Absorption spectra of Ag-decorated ZnO nanocages after CO_2 and complex adsorption using the Hybrid DFT+*U* technique.

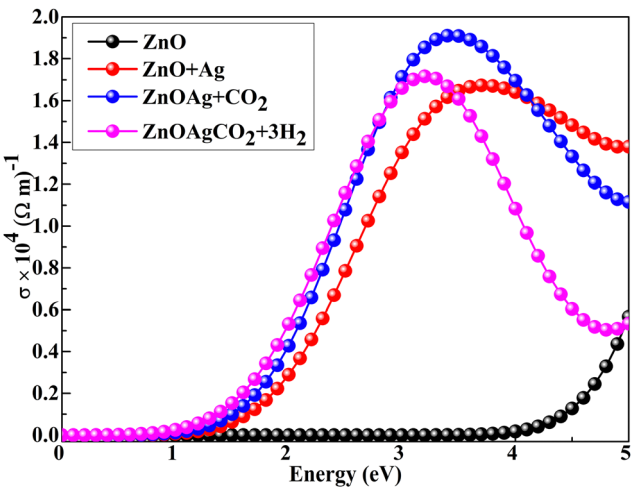

Fig. 7 Optical conductivities of Ag-decorated ZnO nanocages after CO_2 and complex adsorption using the hybrid DFT+*U* technique.

Table 3 Calculated values of electron affinity, ionization potential, Mulliken electronegativity, chemical potential, chemical hardness, chemical softness, electrophilicity index, and charge transfer for the pristine and CO_2-adsorbed ZnO complex

Chemical properties	ZnO	ZnO + Ag	ZnOAg + CO_2	ZnOAgCO_2 + $3H_2$
Ionization energy I (eV)	2.13	−0.01	0.0092	−0.05
Electron affinity A	−1.92	−1.28	−1.24	−0.75
Chemical hardness η	2.03	0.64	0.62	0.35
Chemical softness s $(eV)^{-1}$	0.25	0.79	0.80	1.43
Electronegativity χ (eV)	0.10	−0.65	−0.61	−0.40
Chemical potential μ (eV)	−0.10	0.65	0.61	0.40
Electrophilic index w (eV)	0.01	0.13	0.11	0.03
Charge transfer (ΔN)	—	−0.59	−0.51	−0.30

In a chemical process, electronegativity (χ) refers to the degree to which an element tends to gain electrons and form negative ions,[77] expressed as:

$$\chi = \frac{(IE + Ea)}{2} \quad (10)$$

Chemical potential (μ) refers to an electron's tendency to escape from an equilibrium condition, expressed as:

$$\mu = -\chi \quad (11)$$

Chemical hardness (η) refers to the degree to which a chemical species endures changes in its electronic structure. A change in the chemical hardness, whether positive or negative, affects the stability and reactivity given by the equation.

$$\eta = \frac{(IE - Ea)}{2} \quad (12)$$

Similarly, the reciprocal of chemical hardness (η), known as chemical softness (S), is used to assess the degree of chemical reactivity and depicts an atom or a group of atoms receiving electrons.

$$S = \frac{1}{2\eta} \quad (13)$$

The electrophilicity index (ω) can be used to calculate molecule reactivity.[78]

$$\omega = \frac{\mu^2}{2\eta} \quad (14)$$

The amount of charge transfer between the CO_2 and ZnO nanocages can be obtained as follows:

$$\Delta N = \frac{1}{2} \times \frac{(\mu_{gas} - \mu_{zno})}{(\eta_{gas} - \eta_{zno})} \quad (15)$$

An increase in the higher negative values of ΔN indicates charge transfer from the $(ZnO)_{12}$ nanocage to CO_2 and the complex,[79] as shown in Table 3. The negative value of ΔN affirms that ZnO serves as an electron donor.[80] The negative ionization energy of the CO_2 complex was significantly lower than the positive ionization energy of the CO_2 molecules adsorbed on the surface of the ZnO nanocage, indicating that the complex required more energy than the CO_2 molecule to become a cation. The higher negative electron affinity of the CO_2-adsorbed complex[79] affirmed that it is highly reactive towards electron attraction and releases energy. After the adsorption of CO_2 and the complex on ZnO, the chemical hardness decreased, whereas the chemical softness of the nanocluster material increased. A decrease in hardness indicates a small bandgap value of the nanomaterial, which reduced the species resistance to losing electrons. The adsorption of CO_2 onto the nanocage surface resulted in the softening of ZnO. Negative Mulliken electronegativity values indicate the polar nature of the resulting product. This is supported by the lower hardness values, increased softness, and higher electrophilicity index data in Table 3.[75,81]

4. Conclusion

The structural, adsorption, and optoelectronic properties of the Ag-doped ZnO nanocage in the presence of CO_2 and H_2 gases were systematically investigated using DFT. The Ag atom was adsorbed at the most energetically favorable position, leading to a smaller energy gap and higher conductivity. The electronic properties of the Ag-decorated ZnO were activated by CO_2. A useful byproduct, methanol in (one step), was formed after placing three H_2 molecules in the chemisorbed CO_2 composition. Furthermore, the more negative adsorption energies (−1.76, −0.28, and desorption energy −2.23 eV) increased the sensitivity of the nanocage from 2% to 70% in a short span of time. At 300 K, Ag-decorated $(ZnO)_{12}$ exhibited a maximum sensing response of 54% with a recovery time of 5.06×10^{-09} s. Moreover, temperature changes caused variations in the sensing response. Higher temperatures (330–340 K) did not significantly affect the sensing response but significantly improved the recovery time of the CO_2 gas. Our findings provide useful insights into the fabrication of the novel ZnO-based nanocatalyst for CO_2 activation and conversion to valuable compounds such as methanol.

Author contributions

Shabeer Ahmad Mian, Sheraz Ahmad and Akbar Hussain, modeled the geometry to execute the project and performed a simulation study to obtain all possible data for this study. Sheraz Ahmad, Akbar Hussain, and Shabeer Ahmad Mian analyzed the data, drew the figures, and wrote the manuscript. Sheraz Ahmad, Akbar Hussain and Shabeer Ahmad Mian revised the data and added different temperature-sensing responses and recovery times to the manuscript. Professor Dr Gul Rahman, Shaukat Ali, and Professor Dr Joonkyung Jang assisted with grammatical correction, research theme, and revision and finalization of the manuscript for submission.

Conflicts of interest

The authors declare no competing financial interests but acknowledge competing non-financial interests.

Acknowledgements

This work was supported by the Korea Planning & Evaluation Institute of Industrial Technology and funded by the Korean government (Ministry of Trade, Industry, and Energy, Ministry of Science and ICT, Ministry of the Interior and Safety, National Fire Agency, Project Number 1761002860).

References

1 M. O. Raimi, O. T. Vivien and O. A. Oluwatoyin, *Creating the healthiest nation: Climate change and environmental health impacts in Nigeria: A narrative review*. Morufu Olalekan Raimi, Tonye Vivien Odubo, 2021. 6(4), pp. 12–24.
2 M. P. Baldwin and T. M. Lenton, Solving the climate crisis: Lessons from ozone depletion and COVID-19, *Global Sustainability*, 2020, **3**(9), 29.
3 K. H. Vardhan, P. S. Kumar and R. C. Panda, A review on heavy metal pollution, toxicity and remedial measures: Current trends and future perspectives, *J. Mol. Liq.*, 2019, **290**(22), 111197.
4 A. Antoci, M. Galeotti and S. Sordi, Environmental pollution as engine of industrialization, *Commun. Nonlinear Science Numerical Simulation*, 2018, **58**(13), 262–273.
5 K. H. Vardhan, P. S. Kumar and R. C. Panda, A review on heavy metal pollution, toxicity and remedial measures: Current trends and future perspectives, *J. Mol. Liq.*, 2019, **290**(7), 111197.
6 R. Qadri and M. A. Faiq, Freshwater pollution: effects on aquatic life and human health, *Fresh Water Pollution Dynamics Remediation*, 2020, **1**(2), 15–26.
7 A. K. Singh and R. Chandra, Pollutants released from the pulp paper industry: Aquatic toxicity and their health hazards, *Aquat. Toxicol.*, 2019, **211**(11), 202–216.
8 V. A. Dutkiewicz, *et al.*, Black carbon aerosols in urban air in South Asia, *Atmos. Environ.*, 2009, **43**(10), 1737–1744.
9 I. Manisalidis, *et al.*, Environmental and health impacts of air pollution: a review, *Front. Public Health*, 2020, **2**(4), 14.
10 J. A. Davidson and C. Warren-Gash, Cardiovascular complications of acute respiratory infections: current research and future directions, *Expert Rev. Anti-Infect. Ther.*, 2019, **17**(12), 939–942.
11 A. Agustí and J. C. Hogg, Update on the pathogenesis of chronic obstructive pulmonary disease, *N. Engl. J. Med.*, 2019, **381**(13), 1248–1256.
12 J. A. Neder, *et al.*, Clinical and physiologic implications of negative cardiopulmonary interactions in coexisting chronic obstructive pulmonary disease-heart failure, *Clin. Chest Med.*, 2019, **40**(2), 421–438.
13 S. A. Al Bakheet, *et al.*, Effect of long-term human exposure to environmental heavy metals on the expression of detoxification and DNA repair genes, *Environ. Pollution*, 2013, **181**(2), 226–232.
14 H. Bibi, K. Alam and S. Bibi, In-depth discrimination of aerosol types using multiple clustering techniques over four locations in Indo-Gangetic plains, *Atmos. Res.*, 2016, **181**(4), 106–114.
15 K. Alam, *et al.*, Aerosol optical and radiative properties during summer and winter seasons over Lahore and Karachi, *Atmos. Environ.*, 2012, **50**(7), 234–245.
16 S. A. Twomey, M. Piepgrass and T. Wolfe, An assessment of the impact of pollution on global cloud albedo, *Tellus B*, 1984, **36**(5), 356–366.
17 A. Higurashi and T. Nakajima, Detection of aerosol types over the East China Sea near Japan from four-channel satellite data, *Geophys. Res. Lett.*, 2002, **29**(17), 17-1–17-4.
18 A. Arola, *et al.*, Inferring absorbing organic carbon content from AERONET data, *Atmos. Chem. Phys.*, 2011, **11**(1), 215–225.
19 M. A. Pouresmaeili, I. Aghayan and S. A. Taghizadeh, Development of Mashhad driving cycle for passenger car to model vehicle exhaust emissions calibrated using on-board measurements, *Sustainable Cities Society*, 2018, **36**(3), 12–20.
20 J. Hansen, *et al.*, Global warming in the twenty-first century: An alternative scenario, *Proc. Natl. Acad. Sci. U. S. A.*, 2000, **97**(18), 9875–9880.
21 C. Le Quéré, *et al.*, Global carbon budget 2018, *Earth System Sci. Data*, 2018, **10**(4), 2141–2194.
22 I. U. Din, *et al.*, Revalorization of CO_2 for methanol production via ZnO promoted carbon nanofibers based Cu-ZrO_2 catalytic hydrogenation, *J. Energy Chem.*, 2019, **39**(8), 68–76.
23 K. Ahmad and S. Upadhyayula, *Influence of reduction temperature on the formation of intermetallic Pd2Ga phase and its catalytic activity in* CO_2 *hydrogenation to methanol*, *Greenhouse Gases: Sci. Technol.*, 2019, **9**(3), 529–538.
24 F. Studt, *et al.*, Discovery of a Ni-Ga catalyst for carbon dioxide reduction to methanol, *Nat. Chem.*, 2014, **6**(4), 320–324.
25 X. Zhang, *et al.*, Catalytic conversion of carbon dioxide to methanol: Current status and future perspective, *Front. Energy Res.*, 2021, **8**(2), 413.
26 G. W. Hunter, *et al.*, choice—Critical review—A critical review of solid state gas sensors, *J. Electrochem. Soc.*, 2020, **167**(3), 037570.
27 K. M. Lee, *et al.*, Recent developments of zinc oxide based photocatalyst in water treatment technology: a review, *Water Res.*, 2016, **88**(11), 428–448.
28 M. Kahouli, *et al.*, Structural and optical properties of ZnO nanoparticles prepared by direct precipitation method, *Superlattices Microstruct.*, 2015, **85**(4), 7–23.
29 Y. Li, *et al.*, Formaldehyde detection: SnO2 microspheres for formaldehyde gas sensor with high sensitivity, fast response/recovery and good selectivity, *Sens. Actuators, B*, 2017, **238**(11), 264–273.
30 L. Vayssieres, Growth of arrayed nanorods and nanowires of ZnO from aqueous solutions, *Adv. Mater.*, 2003, **15**(5), 464–466.
31 S.-h Xu, *et al.*, Stability and property of planar (BN) x clusters, *Chem. Phys. Lett.*, 2006, **423**(1–3), 212–214.
32 H. Cao, *et al.*, Well-organized assembly of ZnO hollow cages and their derived Ag/ZnO composites with enhanced photocatalytic property, *Mater. Charact.*, 2020, **160**(8), 110125.

33 A. Wei, L. Pan and W. Huang, Recent progress in the ZnO nanostructure-based sensors, *Mater. Sci. Eng., B*, 2011, **176**(18), 1409–1421.
34 W. Xu, *et al.*, Sensing the cathinone drug concentration in the human body by using zinc oxide nanostructures: a DFT study, *Struct. Chem.*, 2021, **32**(2), 63–68.
35 S. Aslanzadeh, Transition metal doped ZnO nanoclusters for carbon monoxide detection: DFT studies, *J. Mol. Model.*, 2016, **22**(7), 160.
36 M. Kovalenko, *et al.*, A DFT study for adsorption of CO and H_2 on Pt-doped ZnO nanocluster, *SN Appl. Sci.*, 2020, **2**(5), 790.
37 A. Rauf, *et al.*, Tuning the optoelectronic properties of hematite with rhodium doping for photoelectrochemical water splitting using density functional theory approach, *Sci. Rep.*, 2021, **11**(1), 1–11.
38 M. Ilyas, *et al.*, *Tailoring the antifouling agent titanium dioxide in the visible range of solar spectrum for photoelectrochemical activity with hybrid DFT* & DFT+*U approach*, *Mater. Today Commun.*, 2021, **27**(3), 102366.
39 S. Mamoun, A. Merad and L. Guilbert, Energy band gap and optical properties of lithium niobate from ab initio calculations, *Comput. Mater. Sci.*, 2013, **79**(13), 125–131.
40 D. Hamann, H_2O hydrogen bonding in density-functional theory, *Phys. Rev. B: Condens. Matter Mater. Phys.*, 1997, **55**(16), R10157.
41 N. Kaltsoyannis, *et al.*, DFT computation of relative spin-state energetics of transition metal compounds, *Principles*, 2004, **5**(1), 151–184.
42 V. I. Anisimov, F. Aryasetiawan and A. Lichtenstein, First-principles calculations of the electronic structure and spectra of strongly correlated systems: the LDA+U method, *J. Phys.: Condens. Matter*, 1997, **9**(4), 767.
43 V. I. Anisimov, J. Zaanen and O. K. Andersen, Band theory and Mott insulators: Hubbard U instead of Stoner I, *Phys. Rev. B: Condens. Matter Mater. Phys.*, 1991, **44**(3), 943.
44 P. Zhang, *et al.*, Doping effects on the electronic and structural properties of CoO_2: An LSDA+ U study, *Phys. Rev. B: Condens. Matter Mater. Phys.*, 2004, **70**(8), 085108.
45 C. Adamo and V. Barone, Physically motivated density functionals with improved performances: The modified Perdew–Burke–Ernzerhof model, *J. Chem. Phys.*, 2002, **116**(14), 5933–5940.
46 J. Hein and M. Rd, *Improved parallel performance of SIESTA for the HPCx Phase2 system*, Citeseer, 2004, p. 112.
47 M. T. Baei, *DFT Study of* CO_2 *Adsorption on the Zn12O12 Nano-cage*, *Bull. Korean Chem. Soc.*, 2013, **34**(12), 3722–3726.
48 B. O. Kovalenko Mariya, Dzikovskyi Viktor and Bovhyra Rostyslav, A DFT study for adsorption of CO and H2 on Pt-doped ZnO nanocluster, *Appl. Sci.*, 2020, **2**(5), 1–9.
49 J. Cheng, *et al.*, A computational study on the Pd-decorated ZnO nanocluster for H2 gas sensing: a comparison with experimental results, *Phys. E*, 2020, **124**(66), 114237.
50 Sonam, S. Garg and N. Goel, Density functional study on electrochemical reduction of carbon dioxide to C1 products using zinc oxide catalyst, *Theor. Chem. Acc.*, 2023, **142**(3), 31.
51 P. Sikam, *et al.*, *Effect of 3d-transition metals doped in ZnO monolayers on the* CO_2 *electrochemical reduction to valuable products: first principles study*, *Appl. Surf. Sci.*, 2021, **550**(11), 149380.
52 I. Tezsevin, *et al.*, *DFT study on the hydrogenation of* CO_2 *to methanol on Ho-doped Cu (211) surface.* The, *J. Phys. Chem. C*, 2020, **124**(41), 22426–22434.
53 G. Liu, *et al.*, Hydrogen sulfide gas detection by Au-decorated ZnO nanotube: a computational study and comparison to experimental observations, *J. Sulfur Chem.*, 2021, **42**(1), 40–50.
54 R. Shanmugam, A. Thamaraichelvan and B. Viswanathan, Methanol formation by catalytic hydrogenation of CO 2 on a nitrogen doped zinc oxide surface: an evaluative study on the mechanistic pathway by density functional theory, *RSC Adv.*, 2015, **5**(74), 60524–60533.
55 Y. Chen, *et al.*, UV activated hollow ZnO microspheres for selective ethanol sensors at low temperatures, *Sens. Actuators, B*, 2016, **232**(14), 158–164.
56 L. Zhu, *et al.*, Structural stability and ionic transport property of NaMPO4 (M= V, Cr, Mn, Fe, Co, Ni) as cathode material for Na-ion batteries, *J. Power Sources*, 2019, **438**(07), 227016.
57 V. Cretu, *et al.*, Synthesis, characterization and DFT studies of zinc-doped copper oxide nanocrystals for gas sensing applications, *J. Mater. Chem. A*, 2016, **4**(17), 6527–6539.
58 T. M. Abdel-Fattah and M. E. Mahmoud, Selective extraction of toxic heavy metal oxyanions and cations by a novel silica gel phase functionalized by vitamin B4, *Chem. Eng. J.*, 2011, **172**(1), 177–183.
59 A. Hussain, *et al.*, Modulating Optoelectronic and Elastic Properties of Anatase TiO2 for Photoelectrochemical Water Splitting, *Molecules*, 2023, **28**(7), 3252.
60 M. T. Baei, M. B. Tabar and S. Hashemian, $Zn_{12}O_{12}$ fullerene-like cage as a potential sensor for SO_2 detection, *Adsorption Sci. Technol.*, 2013, **31**(5), 469–476.
61 N. L. Hadipour, A. Ahmadi Peyghan and H. Soleymanabadi, Theoretical study on the Al-doped ZnO nanoclusters for CO chemical sensors, *J. Phys. Chem. C*, 2015, **119**(11), 6398–6404.
62 K. Fukui, Role of frontier orbitals in chemical reactions, *Science*, 1982, **218**(4574), 747–754.
63 B. Himmetoglu, *et al.*, Hubbard-corrected DFT energy functionals: The LDA+U description of correlated systems, *Int. J. Quantum Chem.*, 2014, **114**(1), 14–49.
64 A. A. Peyghan and M. Noei, The alkali and alkaline earth metal doped ZnO nanotubes: DFT studies, *Phys. B*, 2014, **432**(77), 105–110.
65 J. Han, P. Mantas and A. Senos, Effect of Al and Mn doping on the electrical conductivity of ZnO, *J. Eur. Ceram. Soc.*, 2001, **21**(10–11), 1883–1886.
66 A. P. Roth, J. B. Webb and D. F. Williams, Band-gap narrowing in heavily defect-doped ZnO, *Phys. Rev. B: Condens. Matter Mater. Phys.*, 1982, **25**(12), 7836.
67 J. Cheng, *et al.*, A computational study on the Pd-decorated ZnO nanocluster for H2 gas sensing: a comparison with experimental results, *Phys. E:*, 2020, **124**(13), 114237.
68 Y.-H. Peng, G.-F. Huang and W.-Q. Huang, Visible-light absorption and photocatalytic activity of Cr-doped TiO2 nanocrystal films, *Adv. Powder Technol.*, 2012, **23**(1), 8–12.

69 M. Kumar, *et al.*, Pd/ZnO nanorods based sensor for highly selective detection of extremely low concentration hydrogen, *Sci. Rep.*, 2017, **7**(1), 1–9.
70 T. R. Anderson, E. Hawkins and P. D. Jones, CO_2, *the greenhouse effect and global warming: from the pioneering work of Arrhenius and Callendar to today's Earth System Models*, *Endeavour*, 2016, **40**(3), 178–187.
71 M. Ren, *et al.*, *Catalytic hydrogenation of* CO_2 *to methanol: a review*, *Catalysts*, 2022, **12**(4), 403.
72 W.-H. Wang, *et al.*, CO_2 *hydrogenation to formate and methanol as an alternative to photo-and electrochemical* CO_2 *reduction*, *Chem. Rev.*, 2015, **115**(23), 12936–12973.
73 S. Y. Bae, *et al.*, Comparative structure and optical properties of Ga-, In-, and Sn-doped ZnO nanowires synthesized via thermal evaporation, *J. Phys. Chem. B*, 2005, **109**(7), 2526–2531.
74 L. Tseng, *et al.*, Green emission in carbon doped ZnO films, *AIP Adv.*, 2014, **4**(6), 067117.
75 S. A. Mian, *et al.*, Molecular Modelling of Optical Biosensor Phosphorene-Thioguanine for Optimal Drug Delivery in Leukemia Treatment, *Cancers*, 2022, **14**(3), 545.
76 Z. Jafari, *et al.*, Potential of graphene oxide as a drug delivery system for Sumatriptan: a detailed density functional theory study, *J. Biomol. Struct. Dyn.*, 2021, **39**(5), 1611–1620.
77 P. Politzer, *et al.*, Average local ionization energies as a route to intrinsic atomic electronegativities, *J. Chem. Theory Comput.*, 2011, **7**(2), 377–384.
78 E. Khan, *et al.*, A theoretical study on molecular structure, chemical reactivity and molecular docking studies on dalbergin and methyldalbergin, *J. Mol. Struct.*, 2019, **1183**(33), 100–106.
79 H.-J. Freund and R. Messmer, *On the bonding and reactivity of* CO_2 *on metal surfaces*, *Surf. Sci.*, 1986, **172**(1), 1–30.
80 X. Zhang, *et al.*, Experimental sensing and density functional theory study of H2S and SOF2 adsorption on Au-modified graphene, *Adv. Sci.*, 2015, **2**(11), 1500101.
81 A. Roya and P. F. Mandana, *Ab initio studies of fullerene effect on chemical properties of naphazoline drop*, 2014.